

Effect of accelerated weathering on physico-mechanical properties of polylactide bio-composites

Moyeenuddin Ahmad Sawpan¹, Muhammad Remanul Islam², Mohammad Dalour Hossain Beg³, Kim Pickering⁴

Abstract In this work, injection moulded hemp fibre reinforced polylactide bio-composites of different fibre contents (0, 10, 20 and 30 wt%) were subjected to accelerated weathering of 12 h cyclic exposures of UV-light at 60°C, water spray and condensation at 50°C for 8, 16, 32, 48 and 64 cycles to study the changes in properties such as crystallinity, tensile, flexural, plane-strain fracture toughness (K_{Ic}) and strain energy release rate (G_{Ic}). The crystallinity of neat polylactide (PLA) was found to increase up to 50.6% after 64 cycles, whereas the crystallinity of composites of different fibre contents was found to increase in the range of 30.6 to 34.5% for 8 to 64 cycles. The overall mechanical properties (tensile, flexural, K_{Ic} and G_{Ic}) of the composites decreased as the number of cycles increased from 8 to 64. The crystallinity and the residual tensile strength, tensile modulus, tensile strain, K_{Ic} and G_{Ic} of the composites of 20 wt% fibres were found to be the highest after 64 cycles. In contrast, the residual flexural strength and flexural modulus of the composites of 30 wt% fibres were found to be the maximum after 64 cycles. Absorption of water, destruction of fibre integrity, degradation of PLA matrix, formation of cracks and pores were found to be the main causes of reduction in the mechanical properties of PLA bio-composites.

Key words Accelerated weathering · Bio-composite · Crystallinity · Hemp fibre · Polylactide

¹ Composite Materials Research, Pultron Composites Limited, Gisborne 4010, New Zealand.

² Section of Chemical Engineering Technology, Malaysian Institute of Chemical and Bioengineering Technology, University of Kuala Lumpur, Alor Gajah-78000, Melaka, Malaysia.

³ Faculty of Chemical and Natural Resources Engineering, Universiti Malaysia Pahang, Gambang-26300, Pahang, Malaysia.

⁴ The University of Waikato, Hamilton 3240, New Zealand.

Corresponding author:

Moyeenuddin Ahmad Sawpan, Composite Materials Research, Pultron Composites Limited, Gisborne 4010, New Zealand. E-mail: moyeen@pultron.com.

Introduction

In recent years, PLA has received significant attention as sustainable alternative to petrochemical based polymers, since the lactide from which it is ultimately synthesized can be produced economically on a mass scale by the bacterial fermentation of carbohydrate rich substances such as corn and potato [1]. For long time PLA based material is being used in biomedical and bioengineering applications such as controlled drug release systems, orthopaedic implant devices and surgical sutures due to its characteristic of biodegradability and biocompatibility. Therefore, a significant research works have been devoted on the study of PLA degradation by varying the environmental factors such as humidity, temperature, pH and enzyme [2-7]. The rate of degradation of PLA also depends on other factors such as molecular weight, crystallinity and crystalline morphology [8, 9].

Potentialities of PLA as a matrix for natural fibre (i.e. lignocellulosic fibre) reinforced bio-composites have been well documented [10-22]. However, knowledge of the factors affecting the degradation mechanism is critical to design the natural fibre reinforced PLA composites with desired life period for different applications. For instance, the resistance to ultraviolet (UV) light is a key factor for most outdoor applications of polymeric materials. The UV-light degradation, also known as photo-degradation, of the polymeric composites of natural fibres ranges from surface discoloration to extensive loss in mechanical properties. The UV-light irradiation can modify and/or degrade the chemical structure of polymer such as molecular chain scission, morphology (breakdown of tie molecules and crystal) and crosslinking [23]. Natural fibre also degrades by UV-light irradiation through free radicals formation and oxidation of phenolic-hydroxyls of lignin. The photo-degradation of lignocellulosic fibre leads to the formation of chromophoric groups, for example carboxylic acids, quinones and hydroperoxy radicals [24, 25].

Many research works have presented influence of various factors such as fibre types [10, 26-28], fibre contents [15, 29, 30], fibre treatment [22, 31], and composite processing [15, 32, 33] on the properties of natural fibre reinforced PLA bio-composites, and some works have reported on the water absorption and durability of PLA bio-composites in different environmental conditions [8, 34-38]. However, very few researches have reported on the accelerated weathering of PLA bio-composites [24, 39].

Testing of composites in real time and in-service environment is not practical because the time involved would significantly delay the product development. Artificial weathering is a very useful technique to evaluate degradation of the natural fibre reinforced composites in a reasonable timeframe. This can be done in an accelerated weathering chamber, where the samples can be exposed to harsh weather conditions including UV-light, condensation, humidity, elevated temperature and rain simulating water spray [24, 39-41]. The objective of this report is to present the effect of accelerated weathering on various properties such as crystallinity, tensile, flexural, K_{Ic} and G_{Ic} of injection moulded PLA composites of different fibre contents (0 to 30 wt%). For this purpose, neat PLA and hemp fibre reinforced PLA composites were aged in an accelerated weathering chamber using UV light, water spray, condensation and heat collectively.

Materials and method

Materials

Poly(lactide 4042D in the form of pellet was obtained from NatureWorks LLC, USA, and hemp fibre was obtained from Hemcore Limited, UK. Chopped dried short hemp fibre (average length 4.9mm) and PLA pellet were

compounded (0, 10, 20 and 30 wt% fibres) using a ThermoPrism TSE-16-TC twin screw extruder. The extruded composites were pelletized and dried at 80°C for 24 h and then injection moulded using a BOY15-S injection moulding machine.

Weathering

Accelerated weathering test was conducted using a QUV panel (Model QUV/spray with solar eye irradiance control). The samples were subjected to 12 h cyclic exposures of UV light, water spray and condensation according to the standard practice for operating fluorescent light apparatus for UV exposure of non-metallic materials, ASTM G154. Each cycle of weathering was comprised of 8 h UV light (340 nm fluorescent UV lamp) exposure at 60°C followed by 0.25 h water spray without light and 3.75 h condensation at 50°C. The samples were exposed for 8, 16, 32, 48 and 64 cycles.

Differential scanning calorimetry (DSC)

The crystallinity of neat PLA and composites was measured using a DSC 2920-TA Instruments machine. All DSC scans were carried out at a scan rate of 10 °C/min from room temperature to 200°C. The sample size was about 10-15 mg. Three repeats of each sample type were performed.

The percent crystallinity (X_{DSC}) of PLA was calculated using Eq. (1) [15]:

$$X_{DSC}(\%) = \left[\frac{(\Delta H_f - \Delta H_{cc}) * 100}{(\Delta H_f^o * w)} \right] \quad (1)$$

where $\Delta H_f^o = 93$ J/g for 100% crystalline PLA, ΔH_f is the enthalpy of melting, ΔH_{cc} is the cold crystallisation enthalpy and w is the weight fraction of PLA in the composite.

X-ray diffraction (XRD)

XRD test of the neat PLA and composites was carried out using a Philips X-ray diffractometer, employing $\text{CuK}\alpha$ ($\lambda = 1.54 \text{ \AA}$) radiation source and a graphite monochromator with a current of 40 mA and a voltage of 40 mV was used with variation of incidence angle from 12° to 45° by 0.030° steps.

Tensile test

Tensile test was carried out according to the standard test method for tensile properties of plastics, ASTM D683. Four specimens of each batch were tested using an Instron 4042 universal test machine. The cross-head speed was 5 mm/min.

Flexural test

Flexural test was conducted using a LLOYD LR 100 K universal testing machine according to the standard test methods for flexural properties of unreinforced and reinforced plastics and electrical insulating materials, ASTM D790. The sample span-to-depth ratio was 16:1, and the cross-head speed was 1.5 mm/min. Four specimens of each batch were flexural tested.

Fracture toughness test

Fracture toughness test was carried out using single-edge-notched-bend (SENB) specimen according to the standard test methods for plane-strain fracture toughness and strain energy release rate of plastic materials, ASTM

D5045. LLOYD LR 100 K universal testing machine was used for this purpose. The Length (L), Span length (S), Width (W) and Thickness (B) of the specimens were 126, 56, 12.7 (± 0.03) and 3.3 (± 0.03) mm respectively, which satisfies the condition $2B < W < 4B$ standardised for SENB specimens used in plane strain fracture toughness of plastics [42]. The initial crack length was 6.35 mm (± 0.005). The loading speed was 10 mm/min and the notch root of the specimens was sharpened using a razor blade before testing. Four specimens of each batch were tested.

Mode I plane-strain fracture toughness (K_{Ic}) of single-edge-notched-bend (SENB) specimen was calculated using Eq. (2):

$$K_Q = (P_Q/BW^{1/2})f(x) \quad (2)$$

where K_Q is the trial K_{Ic} , P_Q is the load, $f(x)$ is the geometrical correction factor ($0 < x < 1$) expressed as a/W and a is the initial crack length. P_Q can be measured from the load versus deformation curve. In this work, K_Q was considered equal to K_{Ic} as reported in [42].

Strain energy release rate (G_{Ic}) was derived from integration of the load versus displacement curve up to the same load point as used for K_{Ic} .

Scanning electron microscopy

Hitachi S-4000 field emission scanning electron microscope was used to study the morphology of the composites. Samples were mounted with carbon tape on aluminium stubs and then sputter coated with platinum and palladium to make them conductive prior to SEM observation.

Optical light microscopy

A Nikon camera (Digital Sight DS-U1) attached to a WILD M3B stereo microscope was used to obtain micrographs.

Results and discussion

DSC analysis

Typical DSC traces of the neat PLA and composites are presented in Fig. 1. The thermograms showed three main successive transitions: (i) glass transition temperature (T_g), the temperature at which a transition between glassy and rubbery states occurred in the amorphous region of PLA, (ii) cold crystallization temperature (T_{cc}), the temperature at which the process of rearrangement of PLA chains occurred to form highly ordered molecular structures (crystallites) when reheated above T_g , (iii) melting temperature (T_m), the temperature at which the crystallites of PLA were melted.

Fig. 2 shows the effect of weathering on the crystallinity (X_{DSC}) and T_g of neat PLA and composites. In Fig. 2a, the crystallinity of unconditioned neat PLA was found to be 7.5% which increased to 14%, a double, for the unconditioned composites of 10 wt% fibres. This was because fibre acted as nucleation site for the crystallisation of PLA [43]. The crystallinity further increased to about 18 and 19% for the unconditioned composites of 20 and 30 wt% fibres, respectively. This was because nucleation sites increased with increased fibre contents [13].

Again in Fig. 2a, the crystallinity of PLA and composites increased with increased number of cycles. The crystallinity of neat PLA was found to increase in the range of 26.1 to 33.2% for 8 to 48 cycles followed by

a sharp rise to 50.6% after 64 cycles. This increment in crystallinity of the neat PLA was attributed to rearrangement of the amorphous PLA chains to highly ordered molecular structures (e.g. spherulites) during the UV-light irradiation cycles at 60°C and condensation at 50°C resulted in cold crystallisation of PLA. Besides, the significant increase in crystallinity could be due to reduction in molecular weight of PLA through degradation upon accelerated ageing [39]. Since the low molecular weight PLA of shorter chains would be more mobile, then the conformational requirement for the ordered crystalline structure would be easier [39]. Other researches [8, 44-46] also showed an increase in crystallinity of neat PLA in the range of 30 to 60% after ageing in different environmental conditions.

Whereas for the composites, the crystallinity increased in the range of 30.6 to 34.5% for 8 to 64 cycles irrespective to fibre contents. Unlike the neat PLA, the crystallinity of composites did not increase significantly from 48 to 64 cycles, which could be due to space limitation in the presence of fibres. After 64 cycles, the crystallinity of composite of 20 wt% fibres was found to be the highest (34.5%). Almost a similar level of increment in crystallinity (38%) of the compression moulded accelerated aged bio-composites of hemp fibre and PLA was reported in other work [24].

In Fig. 2b, T_g of the unconditioned neat PLA was found to be 57.8°C. The aforementioned increased in the range of 61.7 to 64.8°C after weathering for 8 to 48 cycles, which was again due to annealing of amorphous PLA chains during the weathering. Other research work has also reported an increase in T_g of neat PLA due to hydrolytic degradation [47]. Again in Fig. 2b, T_g of the neat PLA disappeared after weathering for 64 cycles. This finding ascribed to degradation of amorphous PLA chains to low molecular weight PLA chains that facilitated to increase the crystallinity as mentioned previously. On the other hand, T_g of the unconditioned composites was obtained in the range of 55.5 to 56.3°C irrespective to the fibre contents. T_g of the unconditioned composites was found to be slightly lower (1.5-2.3°C) than the neat PLA. This decrease in T_g of the composites was due to plasticising effect of the impurities (e.g. wax, pectin, mineral and ash) of hemp fibres [48, 49]. After weathering for 8 to 64 cycles, T_g increased in the range of 59.7 to 62.7°C irrespective to the fibre contents. Above increment in T_g was again due to annealing, and also due to anti-plasticisation phenomenon [50] as a result of leaching of the impurities of hemp fibre during the weathering. Similar to the crystallinity, T_g of the composite of 20 wt% fibres was also found to be the maximum (61.6°C) at 64 cycles.

XRD analysis

Typical XRD diffractograms of the neat PLA is presented in Fig. 3. A broad diffraction hump was observed at the position $16^\circ < 2\theta < 19^\circ$ for the unconditioned neat PLA. This broad hump indicated that PLA chains were poorly ordered (i.e. low degree in crystallinity), which was due to the rapid cooling of PLA during the injection moulding [51]. However, two characteristic crystalline peaks for the neat PLA were observed at the positions 2θ of 16.30° and 18.65° after weathering, which was an indication of crystallisation in neat PLA under the influence of weathering. According to the literatures [52], PLA crystallises as orthorhombic α phase. The 2θ locations for the α phase are established for two diffraction peaks of 16.3° and 18.65° assigned to (200)/(110) and (203) planes, respectively.

In the case of unconditioned composites, just one characteristic crystalline peak of PLA at the position 2θ of 16.40° was observed as shown in Fig. 4a. This crystalline peak was associated to nucleation and crystallisation of PLA in the presence of fibre as discussed in DSC findings. Another major peak was found at the

position 2θ of 22.05° for the composites, which was from the crystalline structure of the cellulose of hemp fibre [53]. In the case of weathered composites in Fig. 4b, the characteristic crystalline peak of PLA at the position 2θ of 18.65° was found once more. This particular finding of crystallites of PLA at the position 2θ of 18.65° was attributed to crystallisation of PLA under the influence of weathering. Other work [39] has also reported crystallites of PLA almost at the same position ($2\theta = 18.70^\circ$) after accelerated weathering of microcrystalline cellulose reinforced PLA composite. Again in Fig. 4b, the characteristic crystalline peak of cellulose was slightly shifted to the position 2θ of 22.40° , which was due overlapping of the two diffraction peaks of cellulose and PLA at the position $22^\circ < 2\theta < 23^\circ$ [22, 54].

Again in Figs. 3 and 4, the intensity of the peaks was found to be increased both for neat PLA and composites after weathering, which was an indication of increase in the degree of crystallinity, a good agreement with the DSC results.

Surface topography of the neat PLA and composites

Fig. 5 presents typical changes such as colour fading and deposition of chalky materials on the neat PLA and composites after weathering. In the case of neat PLA, opacity increased rapidly from 0 to 64 cycles (Fig. 5a). In addition, surface blistering was observed after weathering for 64 cycles (Fig. 5c). The increase in opacity of PLA was due to increase in crystallinity as confirmed through DSC and XRD findings. The surface blistering was a consequence of breakdown of PLA chains through photo-oxidation and hydrolytic degradation. The degradation process of PLA chains through photo-oxidation and hydrolytic reactions are presented schematically in Fig.6. The degradation mechanism of photo-oxidation with UV-light irradiation (Fig. 6a) involves a hydrogen extraction on the PLA chain backbone at the tertiary carbon in the α -position of the ester function followed by formation of macro-radical through reacting with oxygen [55, 56]. The PLA macro-radical then transforms to hydroperoxide by attracting with a labile hydrogen atom which propagates the chain oxidation reaction. Once formed, the hydroperoxide macro-molecule decomposes through β -scission. In the case of hydrolytic degradation (Fig. 6b), the process involves PLA chain cleavage of the ester linkage randomly in amorphous regions to form other compounds such as acid and alcohol through the action of water [4]. This hydrolytic degradation of PLA also leads to an increase in the crystallinity [57, 58].

In addition to blistering, craze and micro-crack were also observed when the neat PLA was weathered for 64 cycles (Fig. 7). The thermal stresses developed as a result of repeated heating through weathering caused to generate extensive multiple crazes, which led to the formation of interpenetrating micro-voids and small fibrils on the surface of neat PLA as evident in Fig. 7a. These micro-voids eventually formed crack as can be seen in Fig. 7b. In addition, erosion of small fibrils in PLA was also occurred as shown in Fig. 7a, which was again due to hydrolytic degradation and photo-oxidation reactions. The formation of crazes in neat PLA as a result of hydration and degradation was also reported in [59].

In Fig. 5b, the typical trend in colour fading from brown to white with respect to cycle number as can be observed for composites. The whitening of composites was again attributed to increased crystallinity of PLA. The colour fading of the composites was also due to UV-degradation of the lignin [60, 61] and leaching of impurities from the hemp fibres. Unlike the neat PLA, surface blistering was not observed for the composites. However, fine white powder was noticed onto the composites after 64 cycles, which was again due to hydrolytic and photo degradations of PLA and hemp fibre.

In Fig. 8, it is evident that the composite specimen did not deform similar to the neat PLA specimen as a result of weathering, which was due to the presence of stiffer lignocellulosic hemp fibre in the PLA matrix. It is well known that hemp fibre is stiffer than PLA matrix as reported in the previous works [15, 48].

Weight changes of the neat PLA and composites

As can be seen in Fig. 9, the weight of neat PLA decreased as the number of cycles increased. This decrease in weight of the neat PLA was due to the loss of materials through erosion and blistering as shown previously. The weight of neat PLA was found to decrease up to 0.33% after 64 cycles. Other works [47, 62, 63] also reported weight loss of the neat PLA as a result of ageing and degradation in different environmental conditions.

Contrarily, the weight of composites initially increased with increased fibre contents as a result of absorption of water during the water spray cycles. It is well known that lignocellulosic materials such as hemp fibre absorbs water because of hydrophilic property [64]. In addition, the number of micro-cracks and debonding in PLA matrix (Fig. 10) increased with increased fibre contents, which was due to differential swelling and shrinkage of fibre and matrix [37, 65]. The micro-cracks facilitated to accumulate more water in the PLA composites of high fibre contents.

Similar to the neat PLA, the weight of composites decreased with increased number of cycles. This weight reduction was due to degradation and loss of materials as evident in Fig. 11 where PLA matrix and fibre were wear out due to weathering. After 64 cycles, the weight of composites was found to increase up to 0.15%, 0.45% and 0.61% for the samples of 10, 20 and 30 wt% fibres, respectively. Other researchers [8, 24, 37, 38] have also found an increase in weight of lignocellulosic fibre reinforced PLA composites due to ageing in wet conditions.

Mechanical properties

The mechanical properties such as tensile, flexural, K_{Ic} and G_{Ic} of the weathered composites are presented in the following sections below. In the case of neat PLA, majority of the specimens was found to deform during the weathering as shown in Fig. 8. [So the mechanical properties of only the control neat PLA are presented in Table 1 as reference.](#)

Tensile properties

Tensile properties such as tensile strength, tensile modulus and tensile strain of the composites with respect to the number of cycles are presented in Fig. 12. As can be observed in Fig.12(a), tensile strength of the composites of 10 and 20 wt% fibres remained approximately stable from 0 to 32 cycles but later substantially decreased as the number cycles increased. Although the load carrying capacity of the composites of 10 and 20 wt% fibres was supposed to deteriorate to some extent due to absorption of water but above calmness in tensile strength at the early stages of weathering was attributed to the greater crystallinity of composites as observed through DSC and XRD findings. The decrease in tensile strength after 48 and 64 cycles was due to deterioration of fibre/matrix interface as a result of degradation of PLA and fibres during the long term weathering. In the case of composite of 30 wt% fibres, the tensile strength gradually decreased from 8 to 64 cycles, which was due to greater absorption of water, degradation of PLA, leaching of materials from the fibre and formation of cracks and pores (Fig. 13). After 64 cycles (i.e. 768 h), the residual tensile strength was found to be 36.8%, 71.3% and 11.86% for the

composites of 10, 20 and 30 wt% fibres, respectively. The superior stability in tensile strength of the weathered composites of 20 wt% fibres was attributed to greater crystallinity and lower water absorption. In the literature [24], the tensile strength of compression moulded PLA and hemp fibre composite was found to be remained up to 13% after accelerated ageing for 1000 h. In another work [39], the tensile strength of microcrystalline cellulose reinforced PLA composite was remained up to 72.6% after accelerated ageing for 200 h. The discrepancies in tensile strength reduction of the above weathered PLA composites were due to variation in reinforcement type and content, degree in crystallinity of PLA, composite processing method and weathering condition.

As can be observed in Fig. 12b, tensile modulus of the composites decreased with increased number of cycles. After 64 cycles, tensile modulus was found to be remained up to 47.3%, 67.2% and 66.7% for the composites of 10, 20 and 30 wt% fibres, respectively. The reduction in tensile modulus was due to weakening in the stiffness of hemp fibres as a result of swelling through absorption of water and destruction of fibre integrity as a consequence of leaching of materials from fibres (Fig. 13). Like the tensile strength, the composite of 20 wt% fibres had the maximum residual tensile modulus after 64 cycles. In Fig. 12c, the tensile strain of composites of 10 and 20 wt% fibres increased slightly in the early stage of weathering (i.e. 8 cycles), afterwards decreased gradually with increased number of cycles. This small increase in tensile strain was attributed to (i) initial steadiness in tensile strength and (ii) decrease in tensile modulus as seen in Fig. 12a and Fig. 12b, respectively. In contrast, the composite of 30 wt% fibres showed a general trend in decrease in tensile strain as the number of cycles increased from 0 to 64 cycles. After 64 cycles, the residual tensile strain was found to be 23.7%, 63.1% and 15.3% for the composites of 10, 20 and 30 wt% fibres, respectively. Again, the composites of 20 wt% fibres had the highest residual tensile strain after 64 cycles, which was consistent with the tensile strength and tensile modulus findings.

Flexural properties

Fig. 14 presents flexural properties such as flexural strength and flexural modulus of the composites with respect to the number of cycles. In Fig 14a, flexural strength of the control (i.e. 0 cycle) samples decreased with increased fibre contents. This behaviour was ascribed to increased stress concentration points (i.e. kinks of fibres and fibre ends) with increased fibre contents [66]. Unlike the tensile strength, flexural strength of the composites of 10 and 20 wt% fibres rapidly decreased just after 8 and 32 cycles, respectively. In the case of composites of 30 wt% fibres, flexural strength decreased steadily from 8 to 64 cycles. After 64 cycles, the residual flexural strength was found to be 31.6%, 41.9% and 69.1% for the composites of 10, 20 and 30 wt% fibres, respectively. In Fig. 14b, flexural modulus of the composites, in general, steadily decreased with increased number of cycles. After 64 cycles, flexural modulus was found to be remained up to 73.7%, 72.6% and 75.4% for the composites of 10, 20 and 30 wt% fibres, respectively. The decrease in both flexural strength and flexural modulus was due to the deterioration of fibre/matrix interface as discuss previously. After 64 cycles, the residual flexural strength and flexural modulus were found to be the maximum for the composites of 30 wt% fibres.

Fracture toughness

K_{Ic} and G_{Ic} results as presented in Fig. 15 indicate the ability of the composites to resist initiation and growth of cracks leading to fracture. In Fig. 15a, K_{Ic} of all the composites was found to increase from 0 to 8 cycles. Afterwards, the composites of 10 and 30 wt% fibres decreased gradually from 8 to 64 cycles. In the case of

composites of 20 wt% fibres, K_{Ic} was remained approximately the same from 8 to 32 cycles and then gradually decreased from 32 to 64 cycles. The initial increase in K_{Ic} was due to arresting of crack propagation as a result of increased toughness promoted by crystallinity [39]. The overall decrease in K_{Ic} from 8 to 64 cycles was due to the formation of pores and cracks as shown previously. As a result of the increase in porosity, more water molecules would be expected to be trapped inside the composite structure, which may have a plasticising effect, resulting in the decrease in K_{Ic} . After 64 cycles, K_{Ic} was found to be remained up to 65.8%, 84.2% and 66.4% for the composites of 10, 20 and 30 wt% fibres, respectively. Like K_{Ic} , G_{Ic} of all the composites also increased but marginally from 0 to 8 cycles. G_{Ic} of the composites of 10 and 30 wt% fibres remained reasonably stable up to 16 cycles and then decreased sharply. On the other hand, G_{Ic} of the composites of 20 wt% fibres marginally decreased from 8 to 64 cycles. After 64 cycles, G_{Ic} was found to be remained up to 38.7%, 63.5% and 43.3% for the composites of 10, 20 and 30 wt% fibres, respectively. The residual K_{Ic} and G_{Ic} of the composites of 20 wt% fibres were found to be the maximum after 64 cycles.

Conclusions

The effect of weathering of UV light, water spray and condensation on the physical and mechanical properties of hemp fibre reinforced PLA bio-composites was investigated in this work. The weight of neat PLA samples was found to decrease due to degradation and loss of materials whereas the weight of composites increased due to absorption of water by the hemp fibres. The shape of the composite specimens was found to be more stable than that of the neat PLA specimens during the weathering. This finding indicated that the structural durability of PLA matrix was improved in the presence of hemp fibre. The crystallinity and T_g were found to increase for both PLA and composites due to rearrangement of the amorphous PLA segments into crystalline phase as a result of cold crystallisation during the weathering. The residual tensile, flexural, K_{Ic} and G_{Ic} of the composites were found to be influenced by the content of fibres. After weathering, the composite of 20 wt% fibres had the highest crystallinity and residual tensile strength, tensile modulus, tensile strain, K_{Ic} and G_{Ic} ; whereas the composites of 30 wt% fibres had the maximum residual flexural strength and flexural modulus. [It can be said that the injection moulded PLA bio-composites of 20 and 30 wt% hemp fibres are promising in terms of durability.](#)

Data availability

The datasets generated during the current study are available from the corresponding author upon request.

Conflicts of interest

The authors declare that there is no conflict of interest regarding the publication of this paper.

References

1. Madhavan Nampoothiri K, Nair NR, John RP (2010) Bioresour Technol 101:8493-8501.
2. Ho K-LG, Pometto AL, Hinz PN (1999) J Environ Polym Degrad 7:83-92.
3. Li S, McCarthy S (1999) Macromolecules 32:4454-4456.
4. Carrasco F, Pagès P, Gámez-Pérez J, Santana OO, MasPOCH ML (2010) Polym Degrad Stabil 95:116-125.
5. Lee SH, Kim IY, Song WS (2014) Macromol Res 22:657-663.
6. Mitchell MK, Hirt DE (2015) Polym Eng Sci 55:1652-1660.

7. Xu L, Crawford K, Gorman CB (2011) *Macromolecules* 44:4777-4782.
8. Ndazi BS, Karlsson S (2011) *eXPRESS Polym Lett* 5:119-131.
9. Owen KL (2013) *Control of microstructure in poly-lactic acid and the effect on biodegradation*: University of Birmingham.
10. Bax B, Müssig J (2008) *Compos Sci Technol* 68:1601-1607.
11. Plackett D, Løgstrup Andersen T, Batsberg Pedersen W, Nielsen L (2003) *Compos Sci Technol* 63:1287-1296.
12. Lee S-H, Ohkita T, Kitagawa K (2004) *Holzforschung* 58:529-536.
13. Mathew AP, Oksman K, Sain M (2005) *J Appl Polym Sci* 97:2014-2025.
14. Wong S, Shanks R (2008) *Compos Interfaces* 15:131-145.
15. Sawpan MA, Pickering KL, Fernyhough A (2011) *Composites Part A* 42:310-319.
16. Pozo Morales A, Güemes A, Fernandez-Lopez A, Carcelen Valero V, De La Rosa Llano S (2017) *Materials* 10: 1286.
17. Gunti R, Prasad AVR, Gupta AVSSKS (2018) *Polym Compos* 39:1125-1136.
18. Asaithambi B, Ganesan G, Ananda Kumar S (2014) *Fibers Polym* 15:847-854.
19. Spiridon I, Darie RN, Kangas H (2016) *Composites Part B* 92:19-27.
20. Graupner N, Müssig J (2017) *Int J Polym Sci* 2017:1-10.
21. Cichorek M, Piorkowska E, Krasnikova N (2017) *J Polym Environ* 25:74-80.
22. Wang F, Zhou S, Yang M, Chen Z, Ran S (2018) *Polymers* 10:401.
23. Shahrudin M, Muhamad F, Zaleha M (2017) *IOP Conf Ser Mater Sci Eng* 165:012021.
24. Islam MS, Pickering KL, Foreman NJ (2010) *Polym Degrad Stabil* 95:59-65.
25. Azwa ZN, Yousif BF, Manalo AC, Karunasena W (2013) *Mater Des* 47:424-442.
26. Siakeng R, Jawaid M, Ariffin H, Sapuan SM (2018) *IOP Conf Ser Mater Sci Eng* 290:012031.
27. Junpeng D, Hongwu W, Wuchang F, Mingyang H (2018) *Polym Compos* 39:E188-E199.
28. Baghaei B, Skrifvars M (2016) *Composites Part A* 81:139-144.
29. Fang W, Mengqing Y, Shujue Z, Siyan R, Junqian Z (2018) *J Appl Polym Sci* 135:46148.
30. Baghaei B, Skrifvars M, Berglin L (2013) *Composites Part A* 50:93-101.
31. Yu T, Ren J, Li S, Yuan H, Li Y (2010) *Composites Part A* 41:499-505.
32. van den Oever MJA, Beck B, Müssig J (2010) *Composites Part A* 41:1628-1635.
33. Baghaei B, Skrifvars M, Salehi M, Bashir T, Rissanen M, et al. (2014) *Composites Part A* 61:1-12.
34. Lee B-H, Kim H-S, Lee S, Kim H-J, Dorgan JR (2009) *Compos Sci Technol* 69:2573-2579.
35. Le Duigou A, Davies P, Baley C (2009) *Polym Degrad Stabil* 94:1151-1162.
36. Siengchin S, Dantungtee R (2013) *J Thermoplas Compos Mater* 26:1424-1440.
37. Gil-Castell O, Badia JD, Kittikorn T, Strömberg E, Martínez-Felipe A, et al. (2014) *Polym Degrad Stabil* 108: 212-222.
38. Hu R-H, Sun M-y, Lim J-K (2010) *Mater Des* 31:3167-3173.
39. Kaynak C, Dogu B (2016) *Int Polym Proc* 31:410-422.
40. Mehta G, Mohanty AK, Drzal LT, Kamdem DP, Misra M (2006) *J Polym Environ* 14:359-368.
41. Beg MDH, Pickering KL (2008) *Polym Degrad Stabil* 93:1939-1946.
42. Pickering KL, Sawpan MA, Jayaraman J, Fernyhough A (2011) *Composites Part A* 42:1148-1156.

43. Mathew AP, Kristiina O, Mohini S (2006) *J Appl Polym Sci* 101:300-310.
44. Paul MA, Delcourt C, Alexandre M, Degée P, Monteverde F, et al. (2005) *Polym Degrad Stabil* 87:535-542.
45. Adam F, Sushant A, Rakesh G (2016) *J Appl Polym Sci* 133:44166.
46. Felfel RM, Hossain KMZ, Parsons AJ, Rudd CD, Ahmed I (2015) *J Mater Sci* 50:3942-3955.
47. Gonzalez MF, Ruseckaite RA, Cuadrado TR (1999) *J Appl Polym Sci* 71:1223-1230.
48. Sawpan MA, Pickering KL, Fernyhough A (2011) *Composites Part A* 42:888-895.
49. Mwaikambo LY, Ansell MP (2006) *J Mater Sci* 41:2483-2496.
50. Moyeenuddin AS (2016) *Polym Compos* 37:3181-3190.
51. Tabi T, Sajo IE, Szabo F, Luyt AS, Kovacs JG (2010) *eXPRESS Polym Lett* 4:659-668.
52. Zhang J, Tashiro K, Tsuji H, Domb AJ (2008) *Macromolecules* 41:1352-1357.
53. Ass BAP, Belgacem MN, Frollini E (2006) *Carbohydr Polym* 63:19-29.
54. Abbate dSF, Cristina VIG, Inês BTM (2017) *Polym Eng Sci* 57:464-472.
55. Gardette M, Thérias S, Gardette J-L, Murariu M, Dubois P (2011) *Polym Degrad Stabil* 96:616-623.
56. Bocchini S, Frache A (2013) *eXPRESS Polym Lett* 7:431-442.
57. Elsayy MA, Kim K-H, Park J-W, Deep A (2017) *Renew Sust Energ Rev* 79:1346-1352.
58. Hakkarainen M, Albertsson A-C, Karlsson S (1996) *Polym Degrad Stabil* 52:283-291.
59. Renouf-Glauser AC, Rose J, Farrar DF, Cameron RE (2005) *Biomaterials* 26:5771-5782.
60. Chaochanchaikul K, Jayaraman K, Rosarpitak V, Sombatsompop PDN (2011) *Bioresources* 7:38-55.
61. Santos RB, Hart P, Jameel H, Chang H-m (2013) *Bioresources* 8:1478-1507.
62. Delabarde C, Plummer CJG, Bourban P-E, Månson J-AE (2011) *Polym Degrad Stabil* 96:595-607.
63. Guralp O, Sebnem K (2009) *J Appl Polym Sci* 114:2481-2487.
64. Sair S, Oushabi A, Kammouni A, Tanane O, Abboud Y, et al. (2018) *Case Stud Constr Mater* 8:203-212.
65. Thwe MM, Liao K (2003) *Compos Sci Technol* 63:375-387.
66. Sawpan MA, Pickering KL, Fernyhough A (2012) *Composites Part A* 43:519-526.

Captions of figures

Fig. 1 Typical DSC thermograms of the neat PLA and composites.

Fig. 2 (a) Crystallinity (X_{DSC}) and (b) glass transition temperature (T_g) of the neat PLA and composites at different cycle numbers.

Fig. 3 XRD diffractograms of the unconditioned and weathered neat PLA.

Fig. 4 Typical XRD diffractograms of (a) unconditioned and (b) weathered composites (20 wt% fibres).

Fig. 5 Photographs of (a) weathered neat PLA (b) weathered composites (20 wt% fibres) and (c) surface blistering of neat PLA. The numbers in parentheses indicate the weathering cycle numbers.

Fig. 6 Reaction schemes of (a) photo-oxidation and (b) hydrolysis of neat PLA.

Fig. 7 Light microscope images of 64 cycles weathered neat PLA showing (a) craze and erosion (in circle) and (b) crack (indicating by arrows).

Fig. 8 Deformation and stability of neat PLA and composite, respectively.

Fig. 9 Changes in the weight of neat PLA and composites with respect to number of cycles.

Fig. 10 (a) Light microscope image and (b) SEM micrograph of the composite of 30 wt% fibres after 64 cycles showing micro-cracks and fibre/matrix debonding.

Fig. 11 SEM micrograph of the composite of 20 wt% fibres after 64 cycles showing degradation and materials losses.

Fig. 12 (a) Tensile strength, (b) tensile modulus and (c) tensile strain of the composites with respect to the number of cycles.

Fig. 13 SEM micrograph of the composite of 30 wt% fibres after 64 cycles showing leaching of materials from fibres, degradation of PLA, cracks and pores.

Fig. 14 (a) Flexural strength and (b) flexural modulus of the composites with respect to the number of cycles.

Fig. 15 (a) K_{Ic} and (b) G_{Ic} of the composites with respect to the number of cycles.

List of table

Table 1 Mechanical properties of the neat PLA

Fig. 1

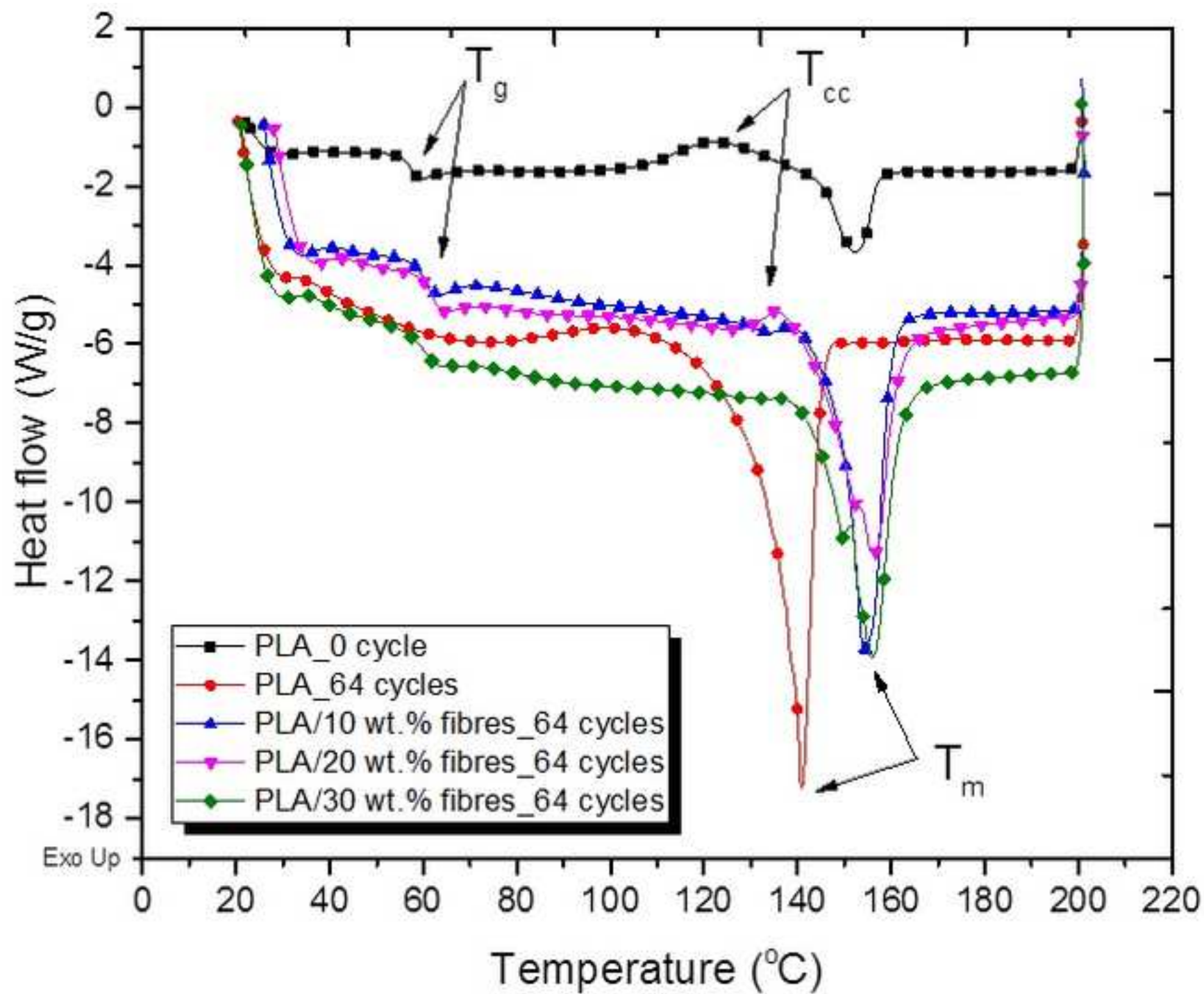


Fig. 2

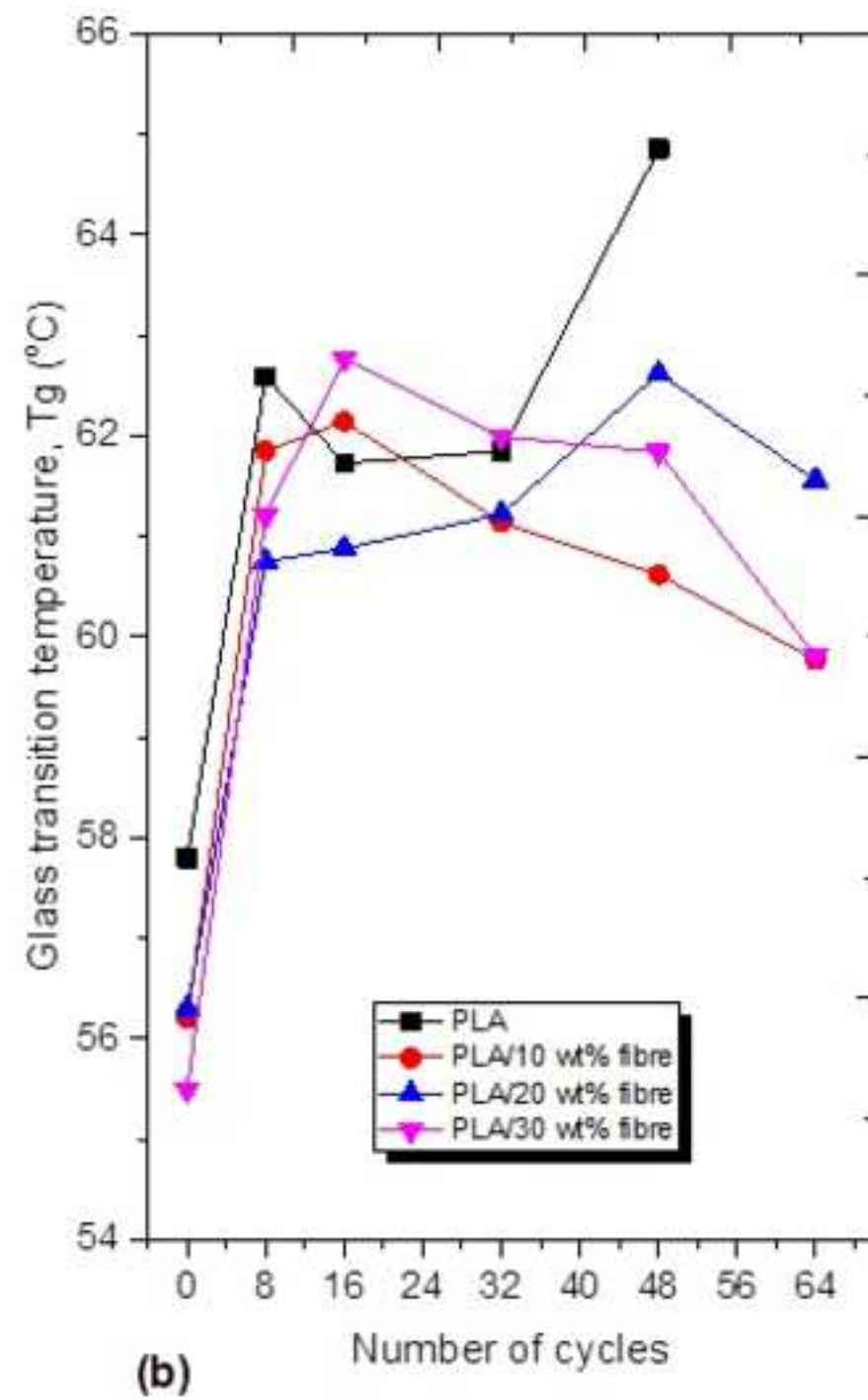
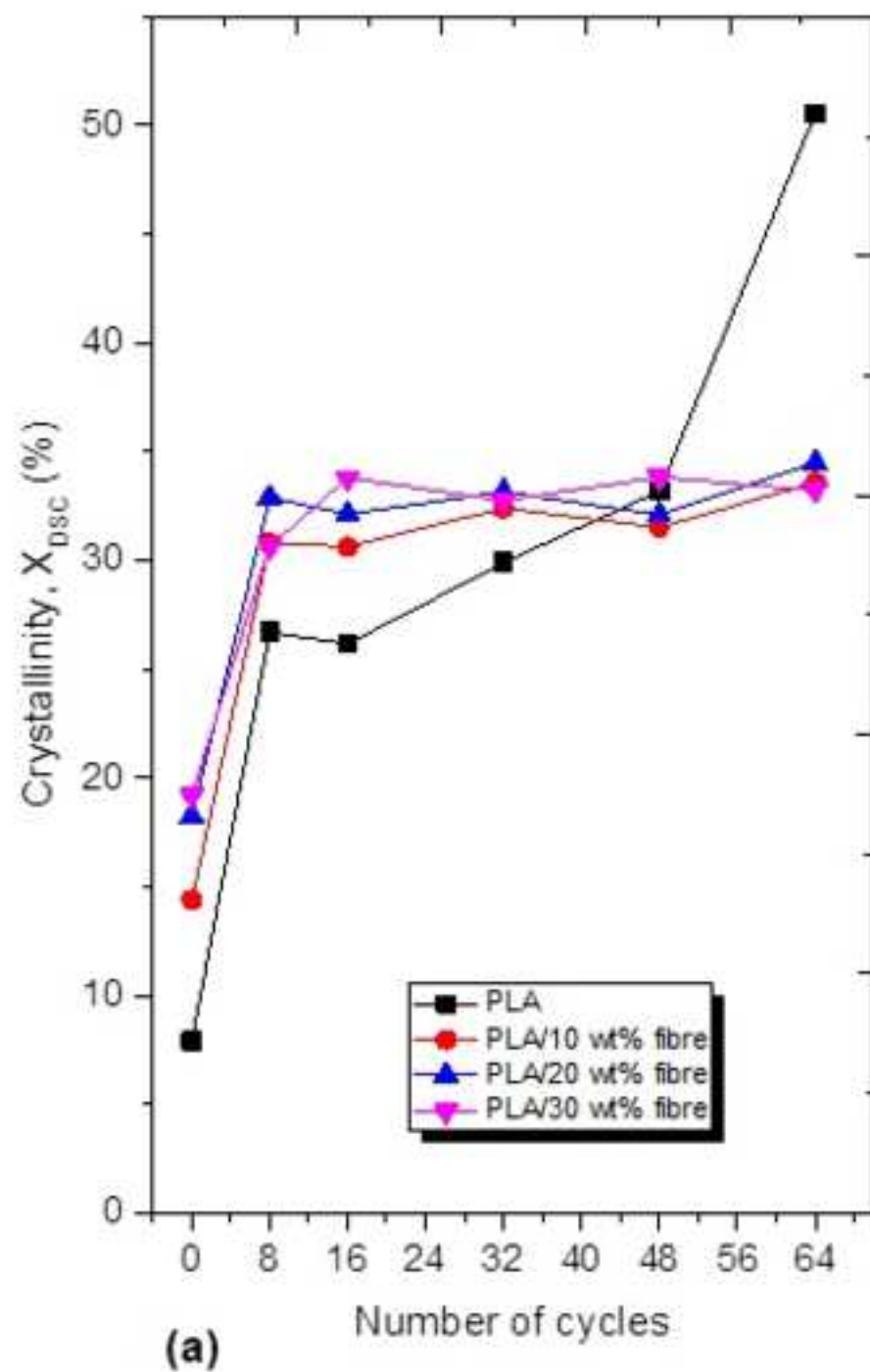


Fig. 3

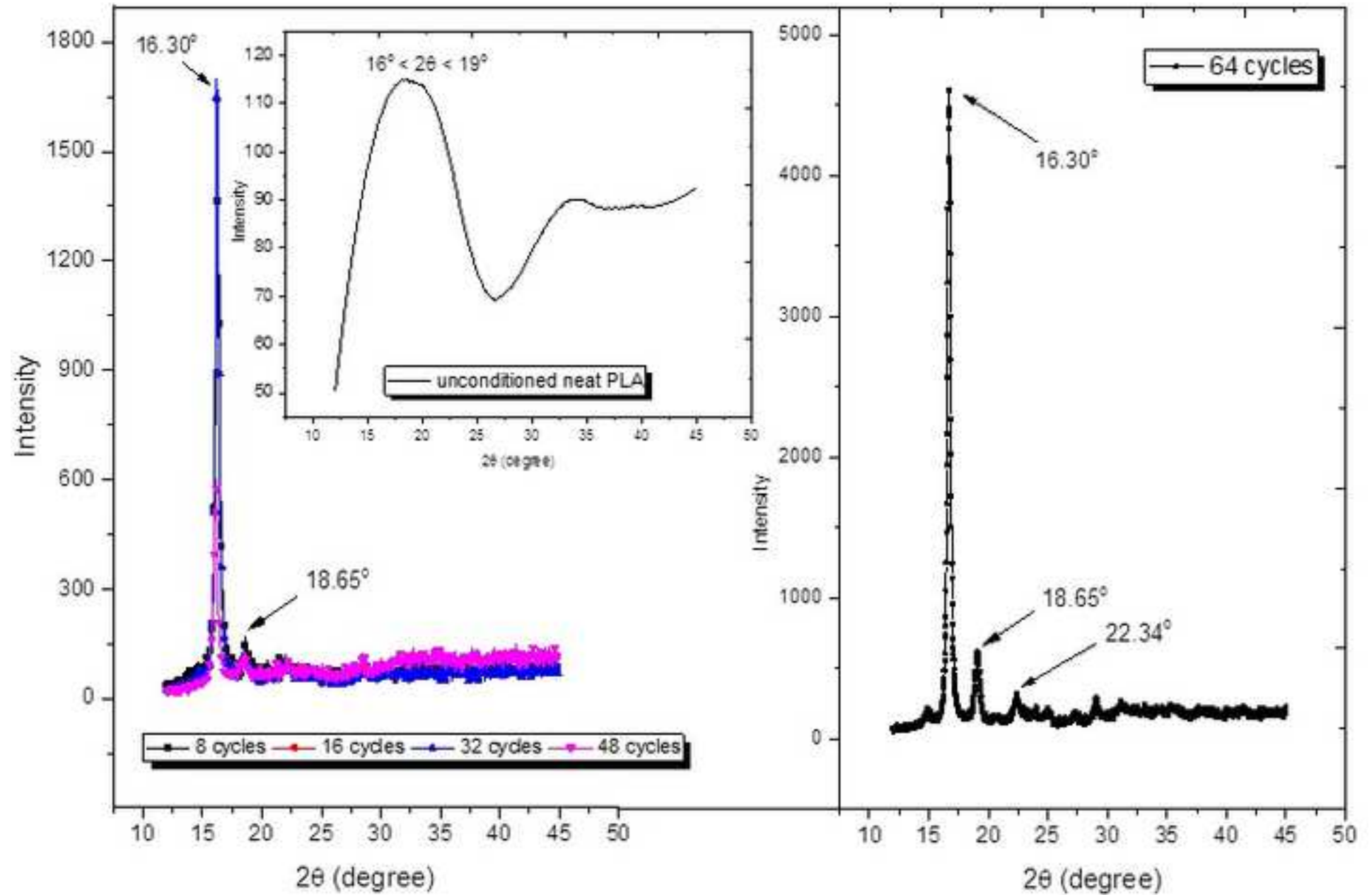
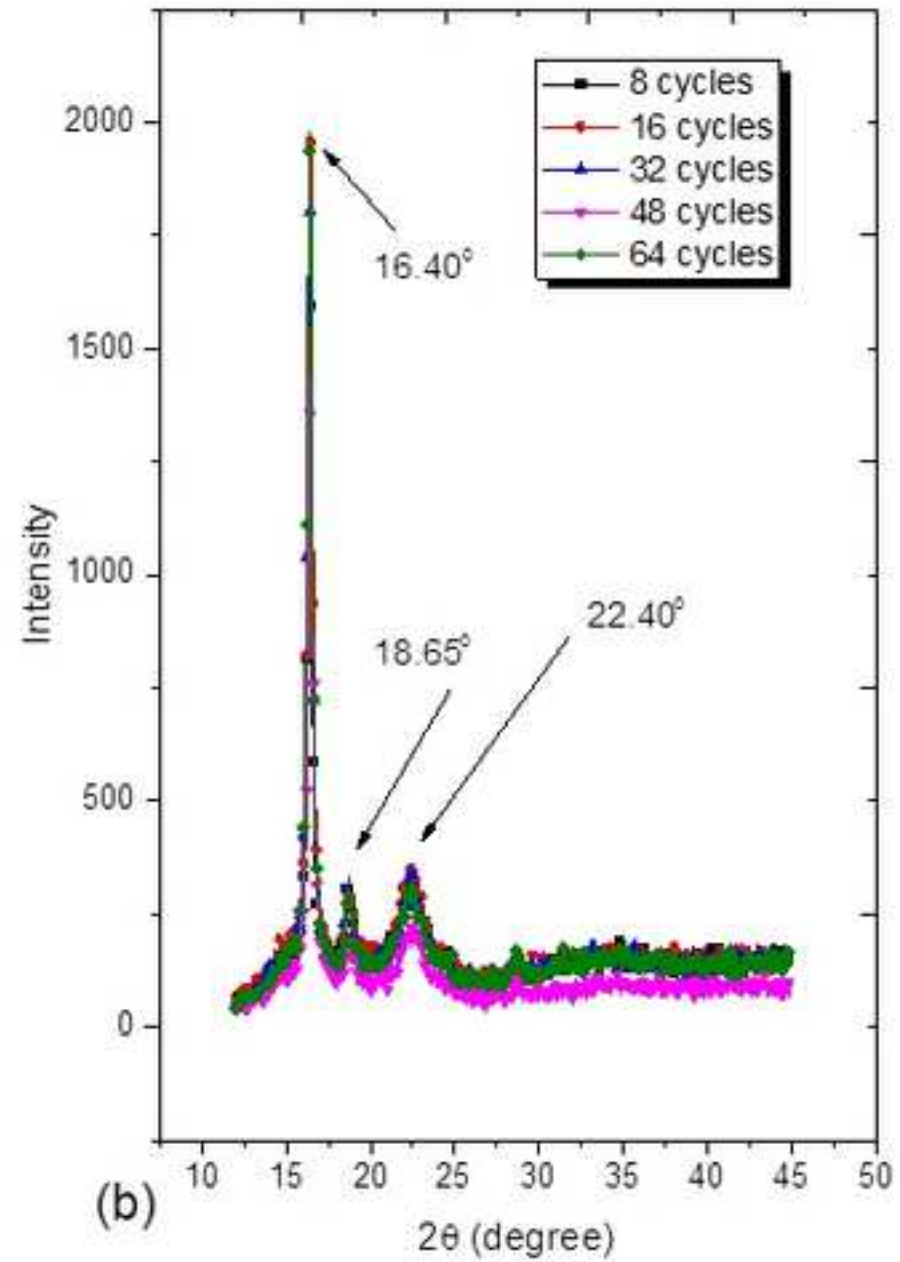
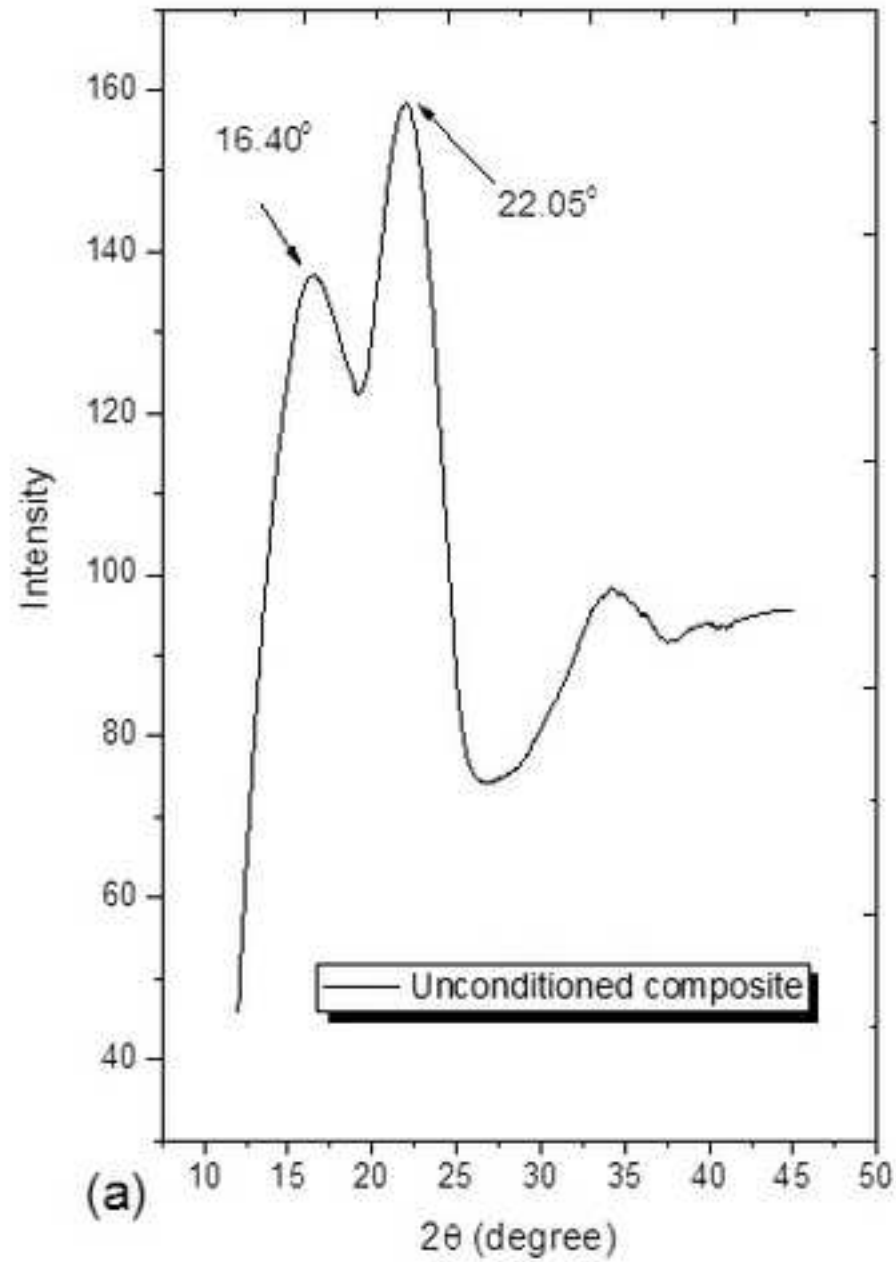
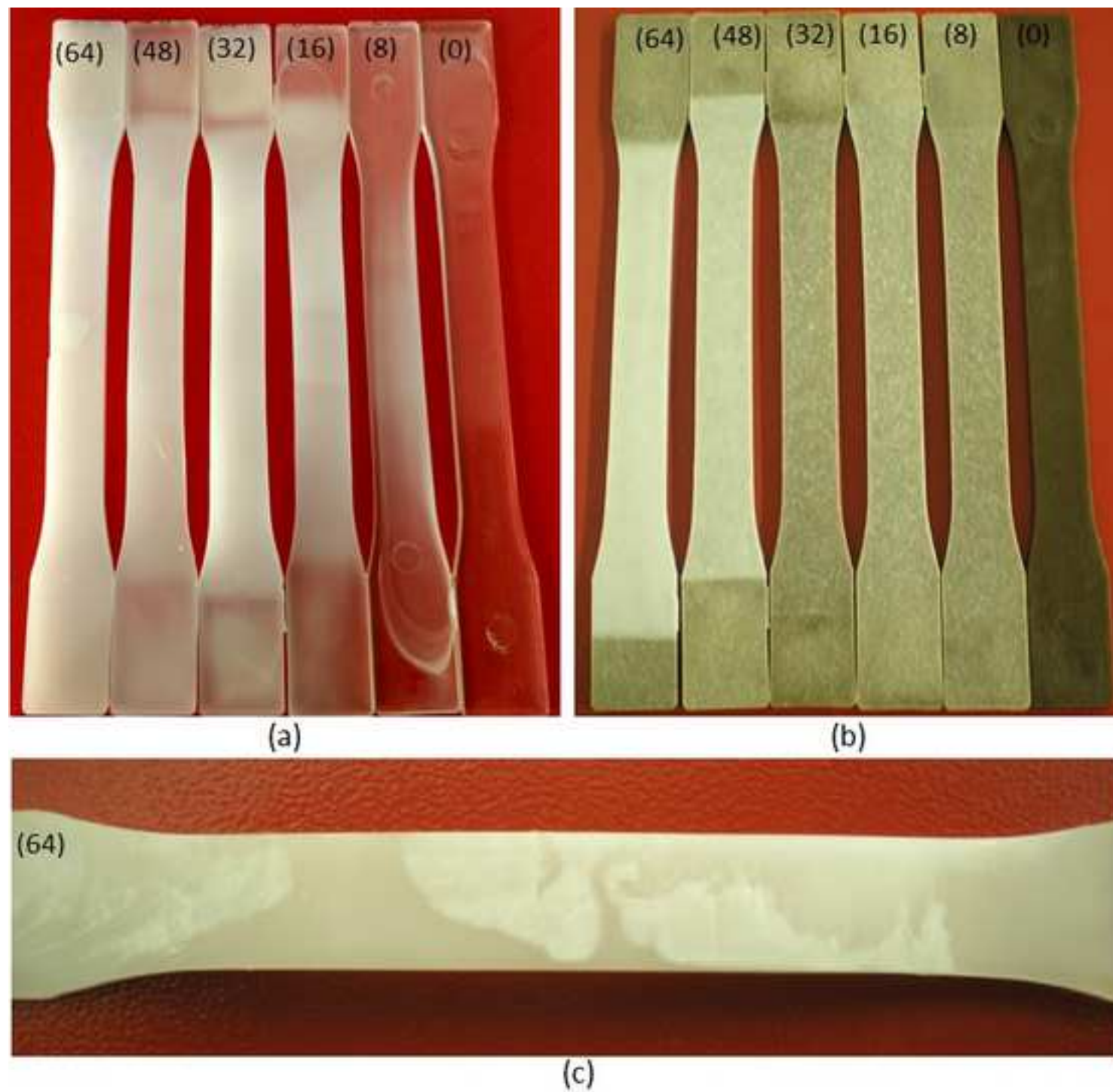
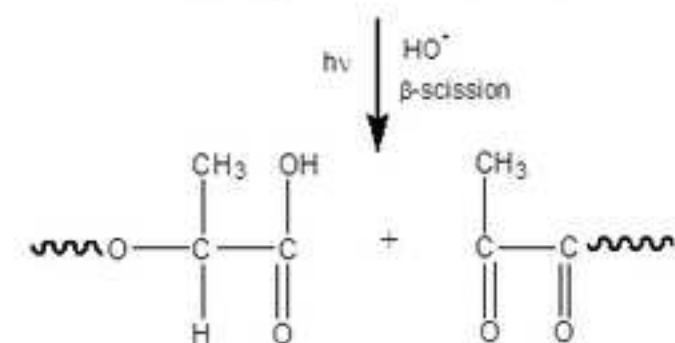
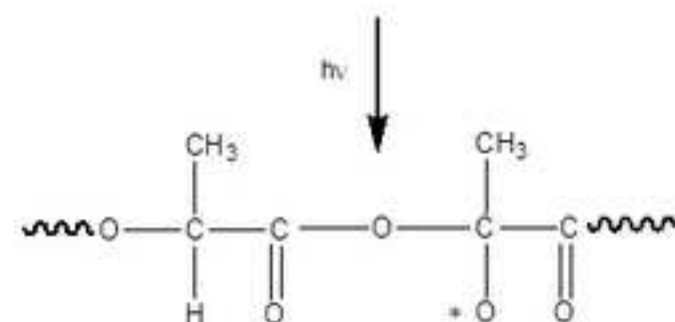
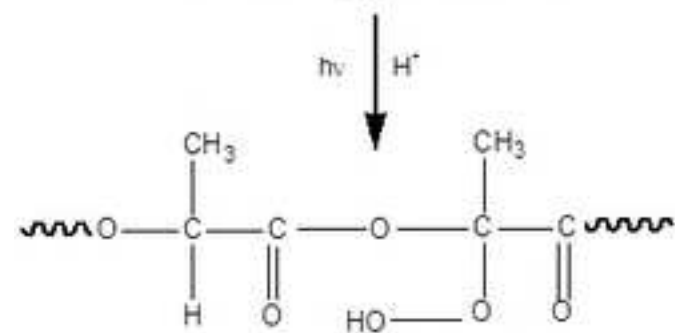
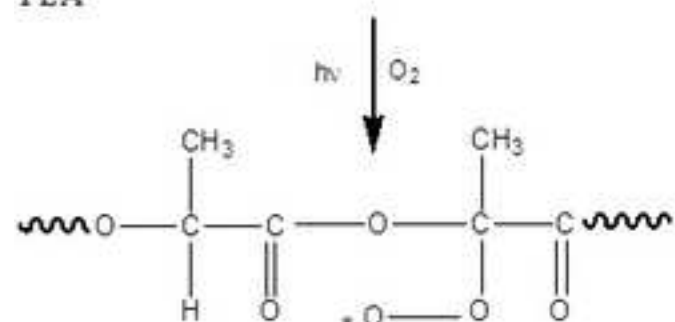
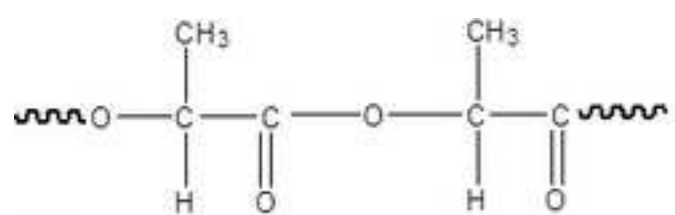


Fig. 4



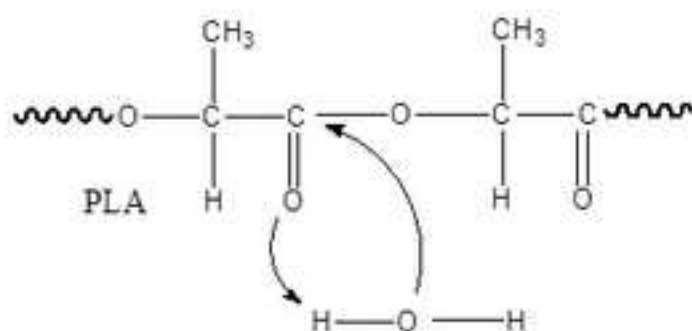




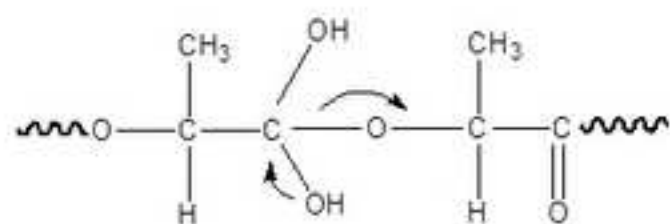
Carboxyl end group

Diketones

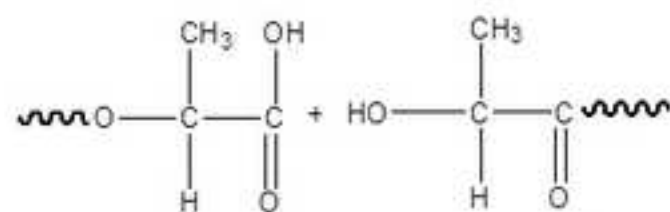
(a)



Hydrolysis



Degradation



Carboxyl end group

Hydroxyl end group

(b)

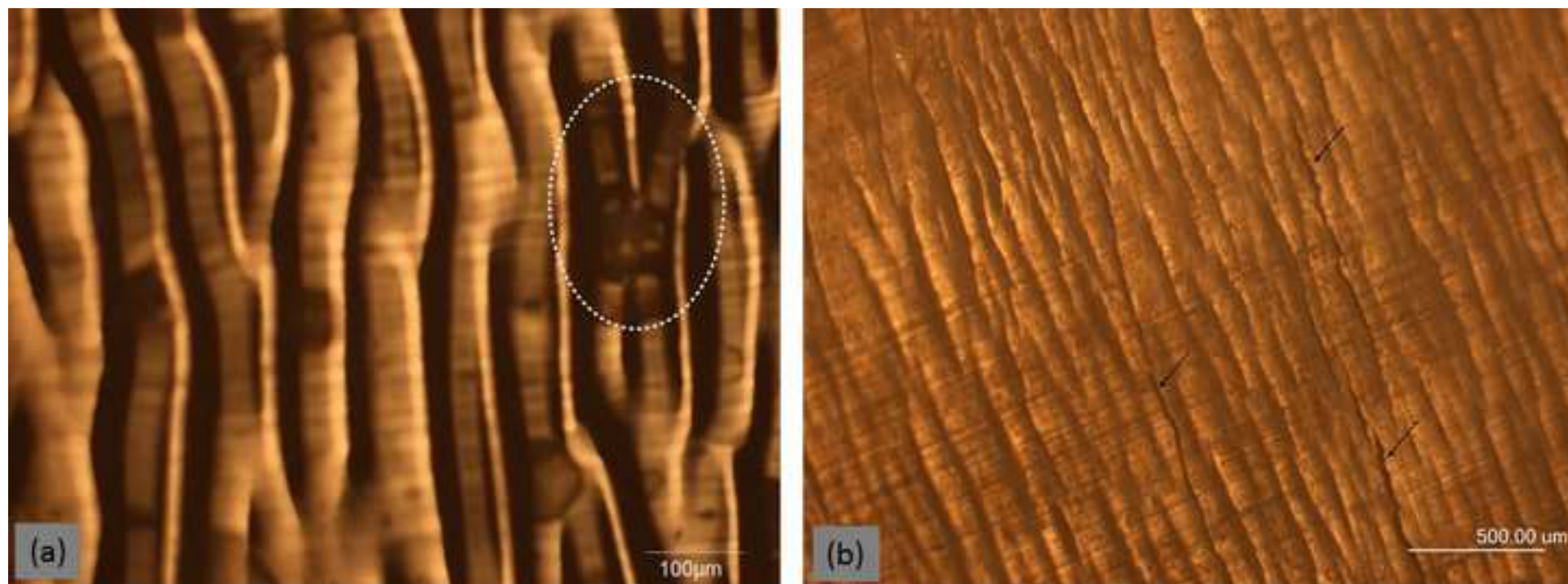
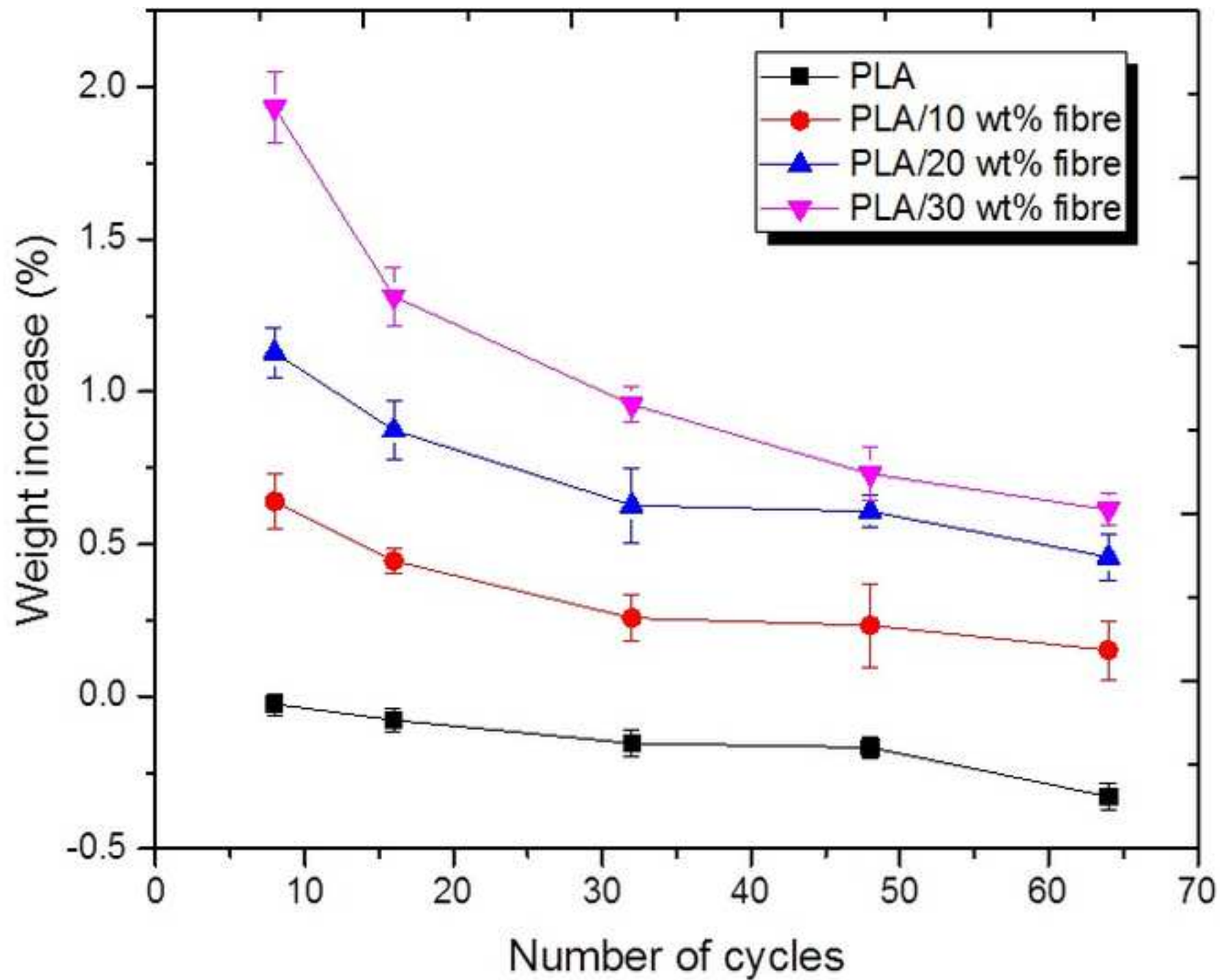
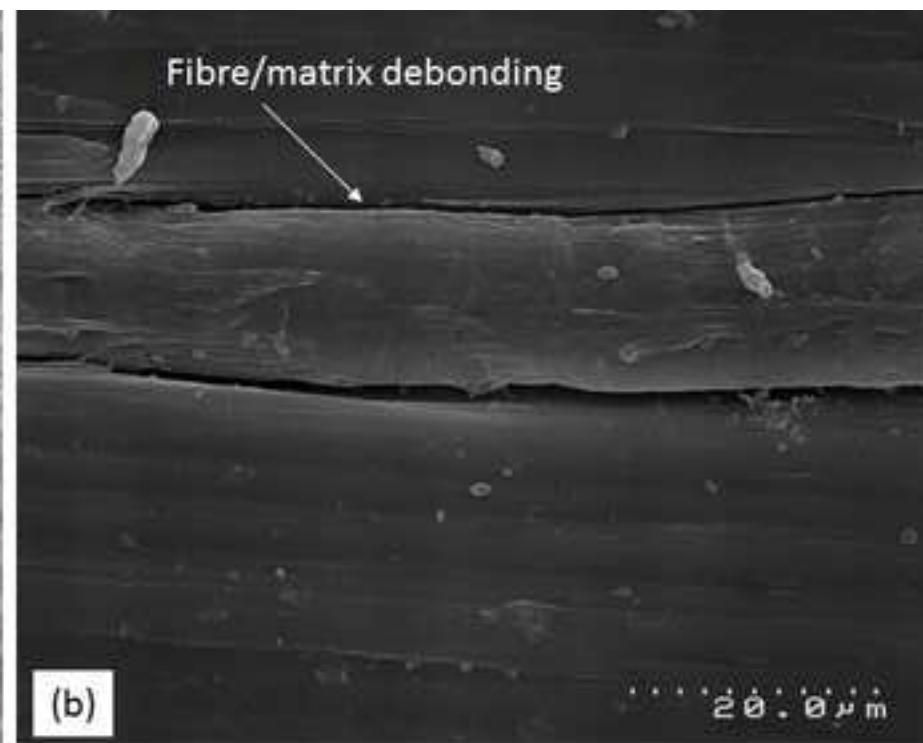
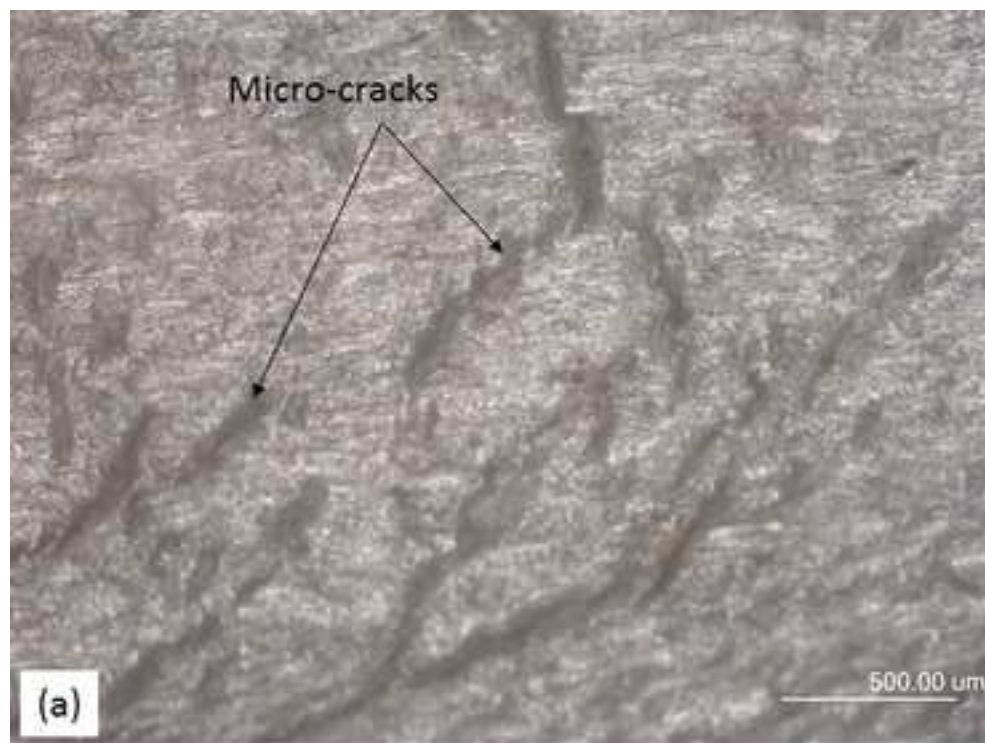
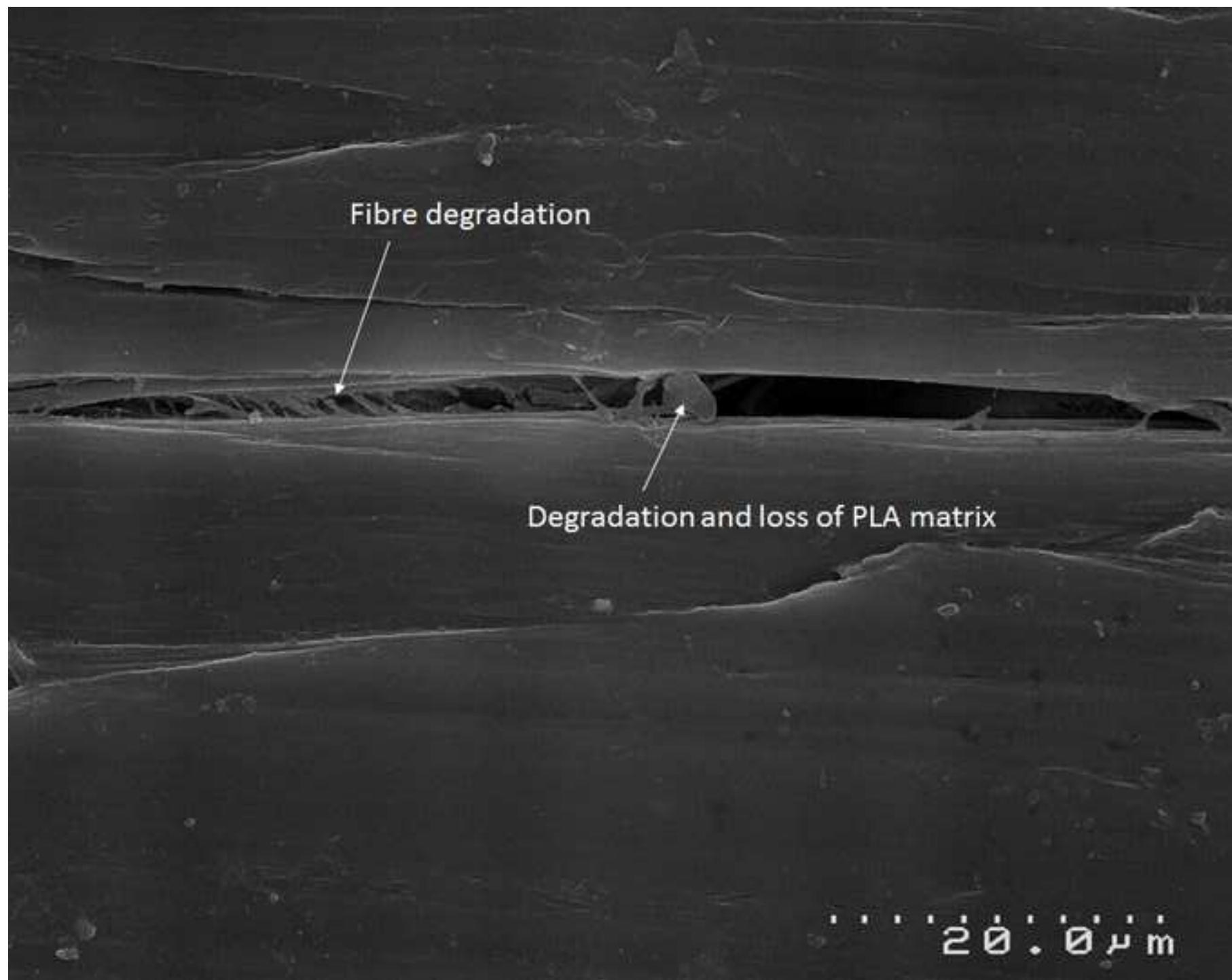


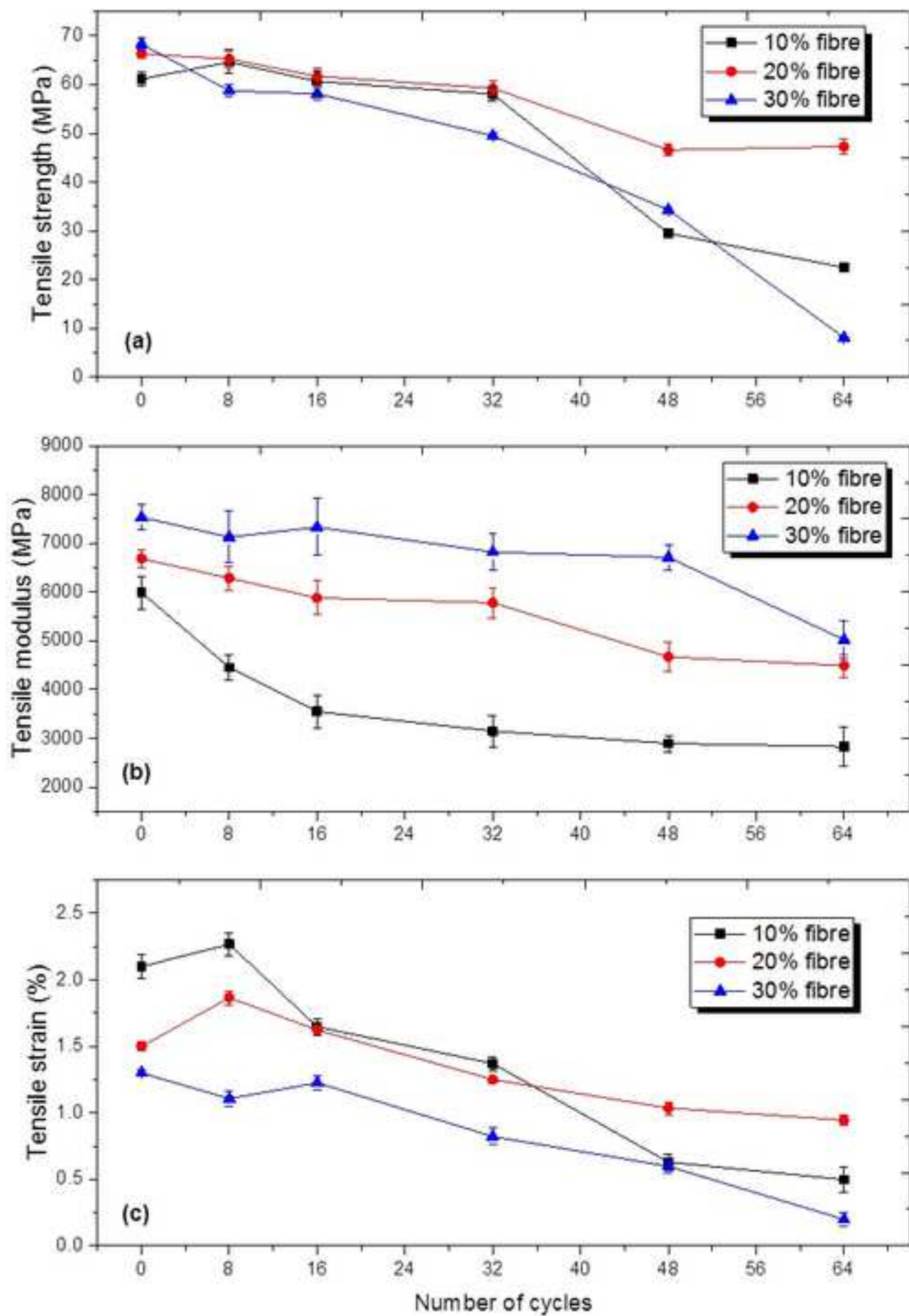


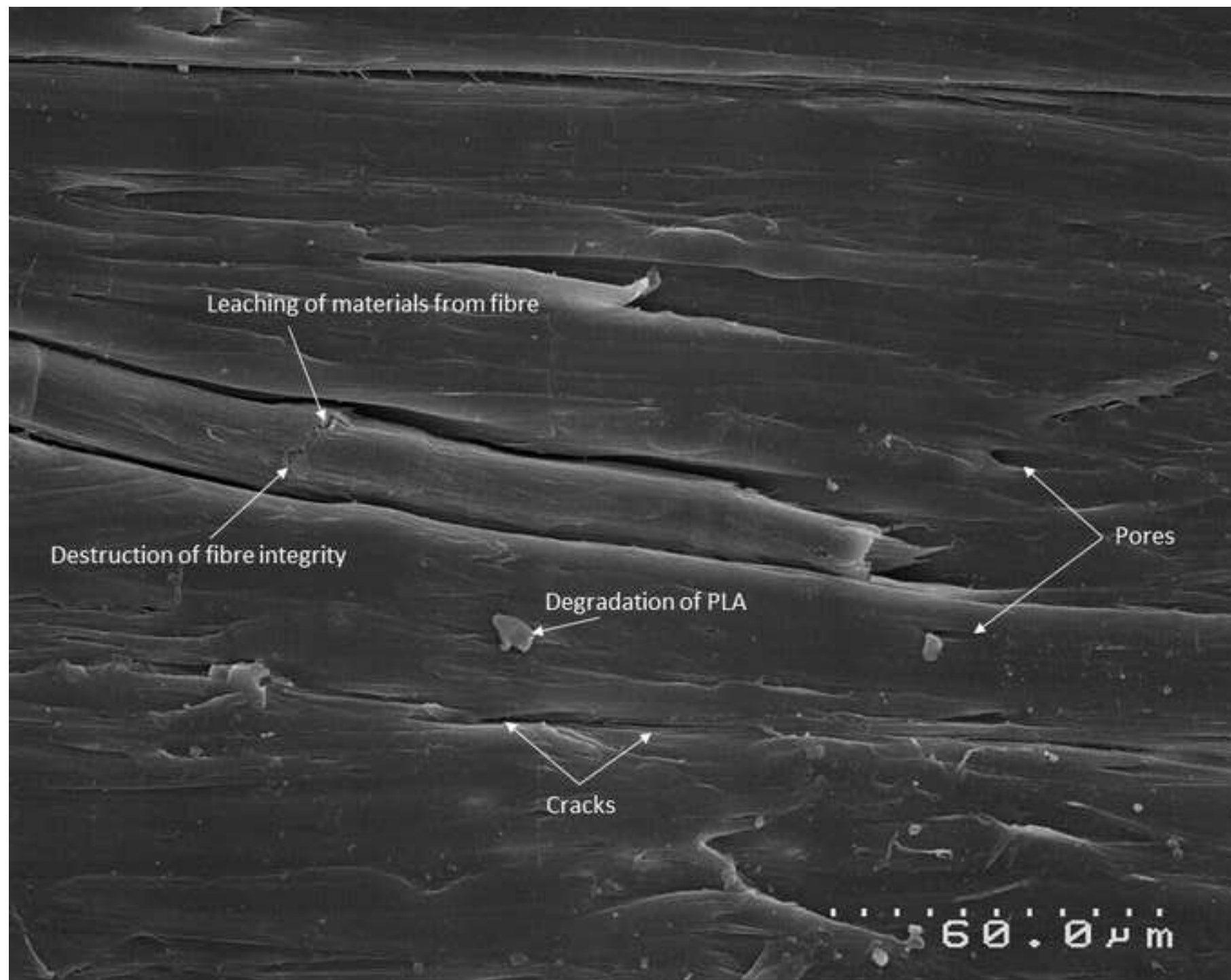
Fig. 9

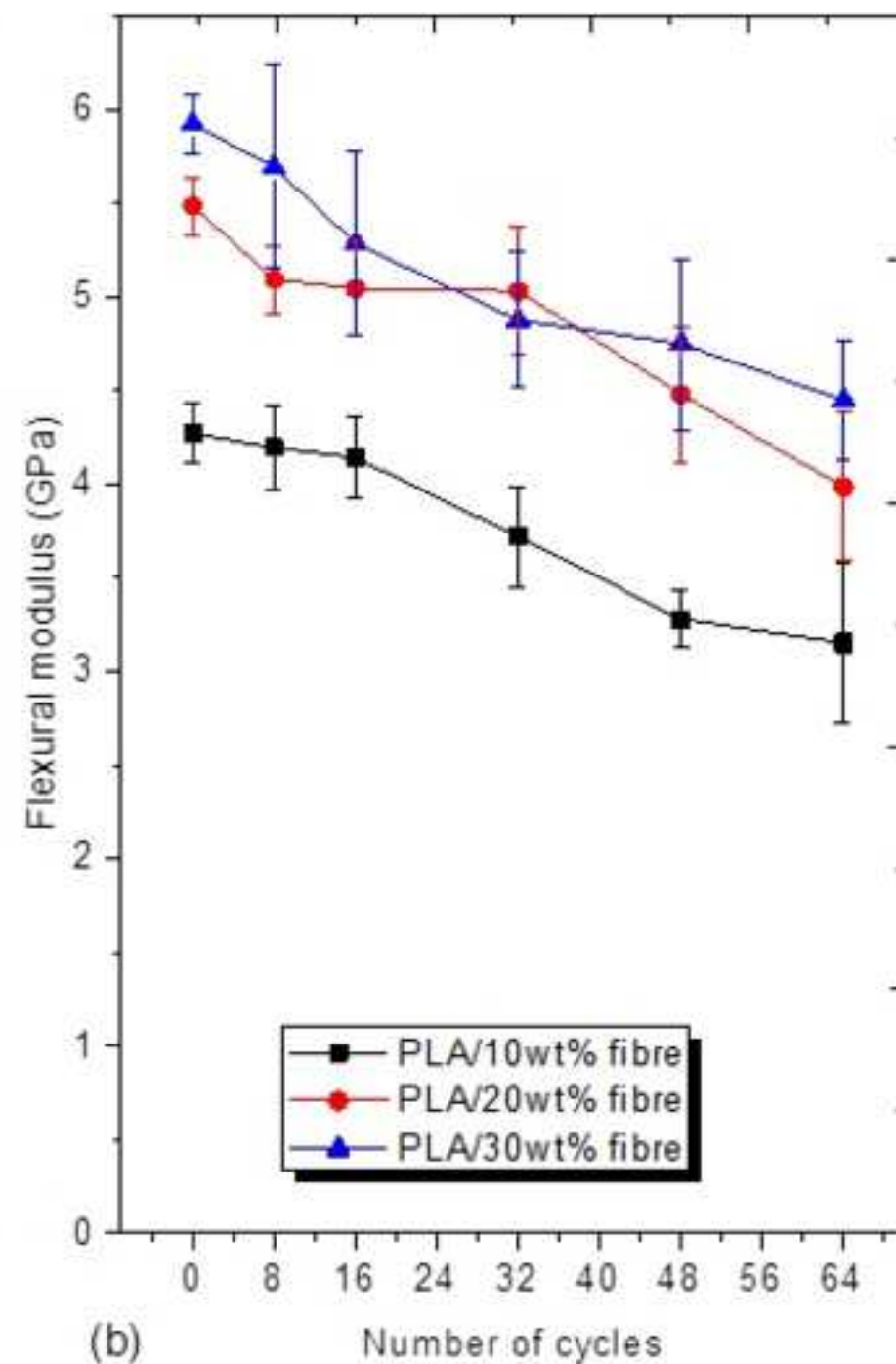
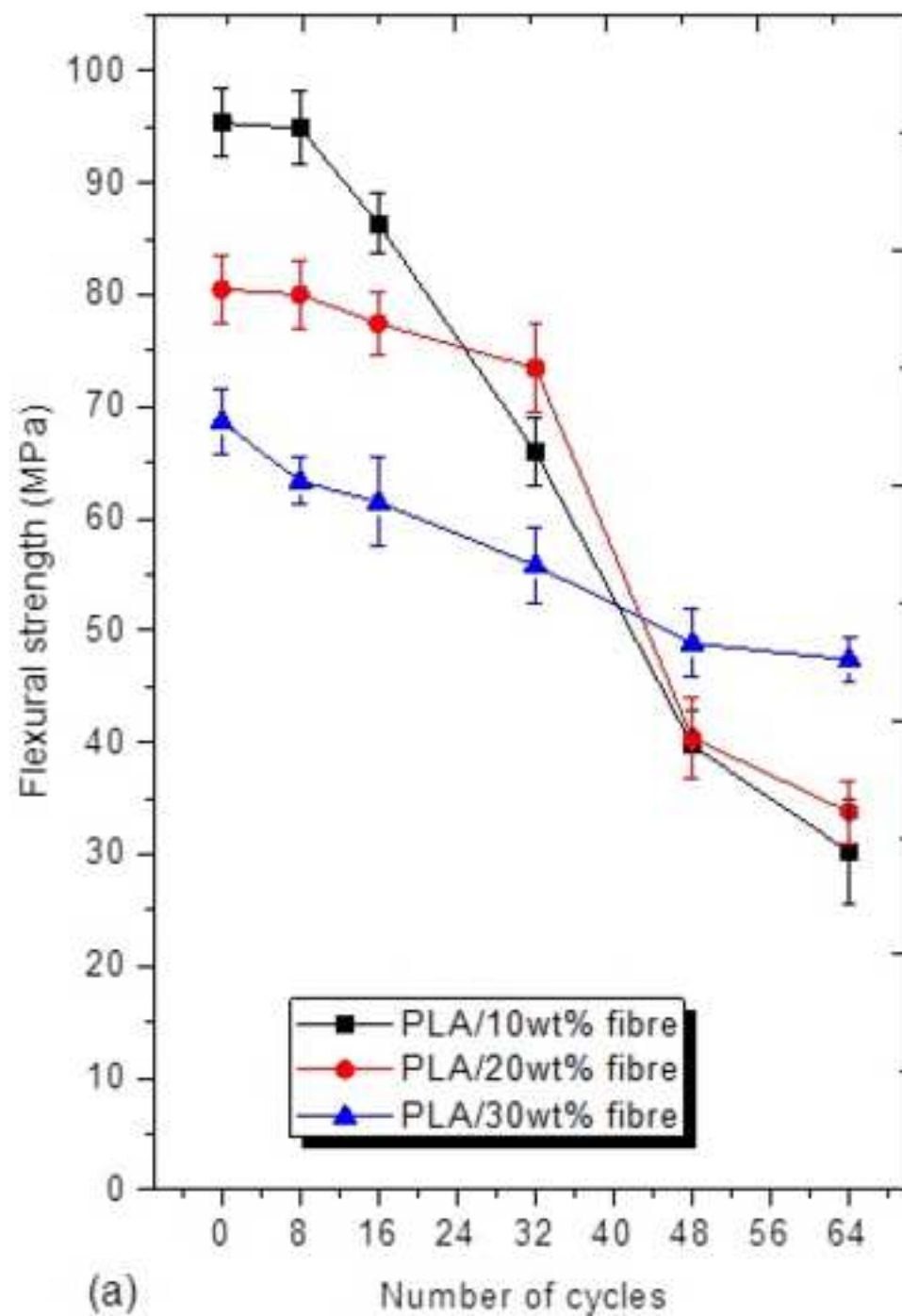












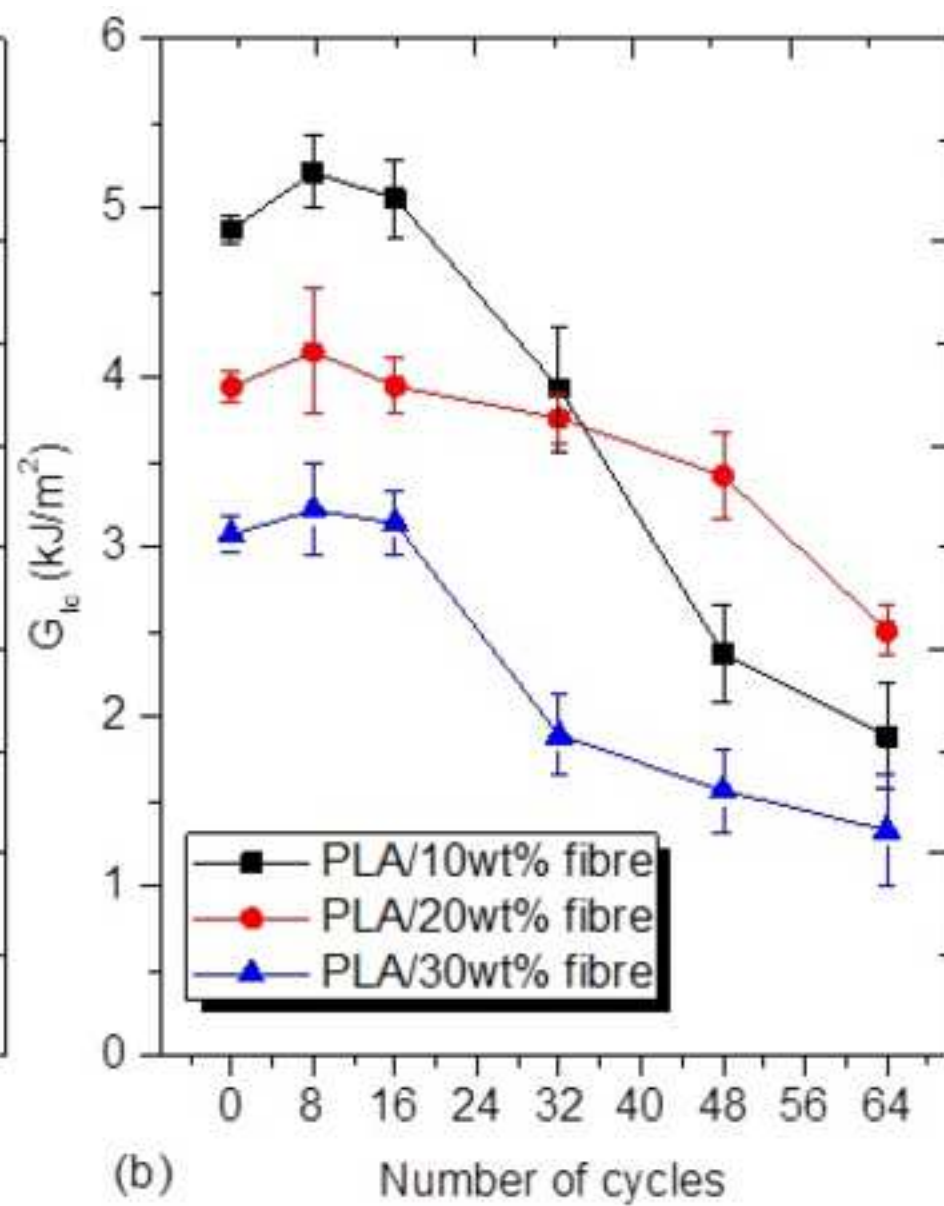
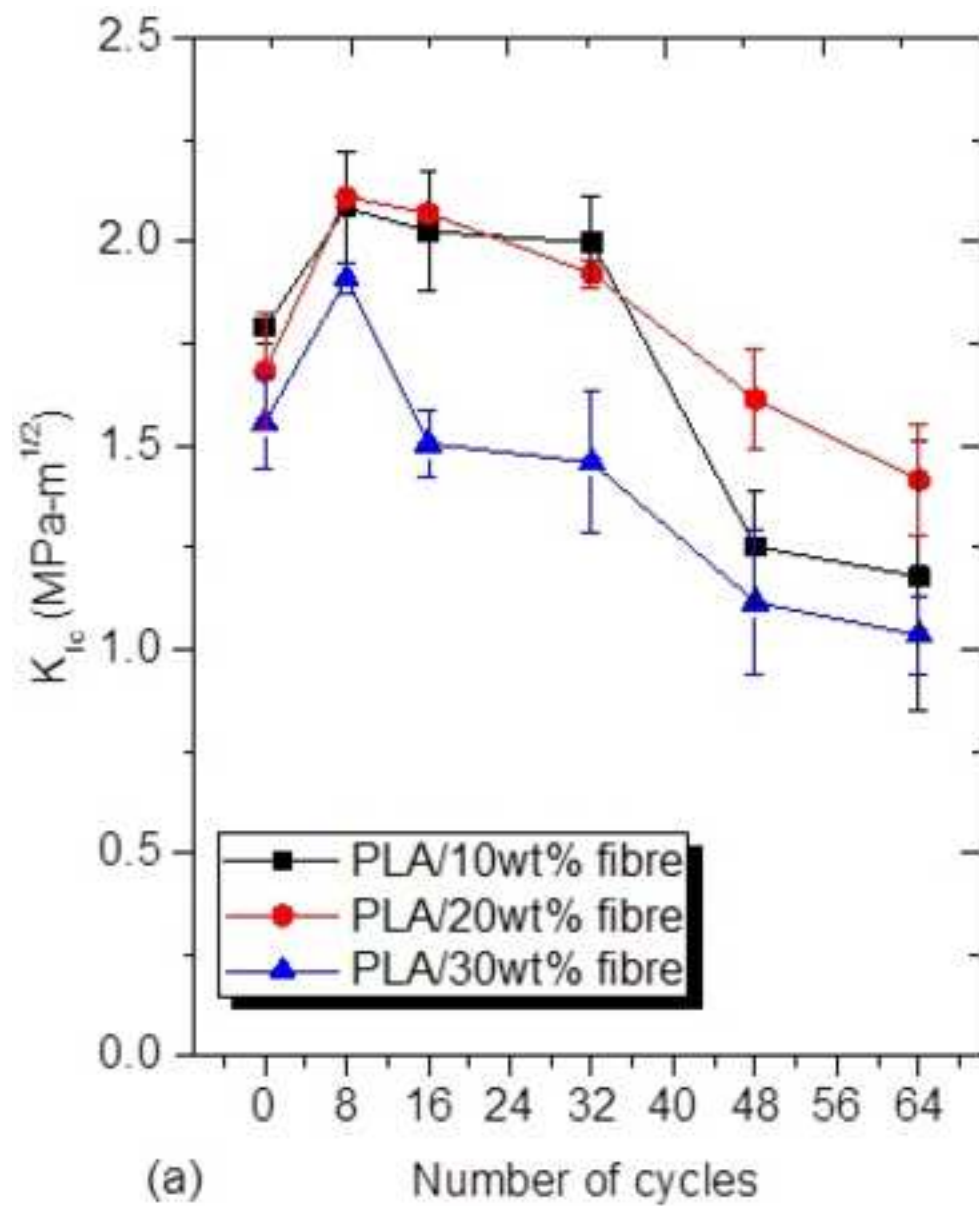


Table 1 Mechanical properties of the neat PLA

Properties	Values
Tensile strength (MPa)	50.8 (± 1.21)
Tensile modulus (GPa)	3.50 (± 0.20)
Tensile strain (%)	3.05 (± 0.19)
Flexural strength (MPa)	96.01 (± 3.01)
Flexural modulus (GPa)	3.40 (± 0.15)
K_{Ic} (MPa·m ^{1/2})	2.02 (± 0.09)
G_{Ic} (kJ/m ²)	6.11 (± 0.06)